PBPC ISSN 2674-9432
Qualis A3 CAPES 2021-2024 | DOI - Crossref | Latindex | Indexado no Google Acadêmico

NUMERICAL EVALUATION OF SCALE-INHIBITOR DISTRIBUTION IN ANNULAR TWO-PHASE FLOW FOR AN OFFSHORE PRODUCTION PIPELINE

Nathália Melo Roseane de Melo, Deisiane Santos Oliveira, Anderson Viana do Nascimento, Rebeca Nicolle da Silva, Ellen Raisa Machado de Lima, Fernanda Lira, Giselle Maria Lopes Leite da Silva, Tiago Cavalcante Freitas, Paulo Roberto Maciel Lyra, Alessandro Romário Echevarria Antunes, Darlan Karlo Elisiário de Carvalho

https://doi.org/10.36557/2674-9432.2026v5n3p2845-2864
Artigo recebido em 28 de Março e publicado em 28 de Maio de 2026

ORIGINAL ARTICLE

RESUMO

This study presents, for the first time in the literature, a numerical investigation of the dispersion of a scale inhibitor, which uses monoethylene glycol (MEG) as a solvent, injected into oil-production pipelines operating under oil–water core-annular flow conditions. The proposed methodology combines 1D simulations with 3D simulations. The prediction of flow conditions such as pressure, temperature, holdup, and flow pattern profiles throughout the production line was performed using the transient 1D multiphase flow simulator ALFAsim. The results of the 1D simulation were used as boundary conditions for 3D simulations performed in ANSYS Fluent to characterize the local multiphase flow near the Chemical Injection Valve (CIV). Four injection scenarios were evaluated based on nominal manufacturer rates and real field-measured rates. The simulations reveal that the injected inhibitor remains confined to the water layer throughout the domain. Near the injection region, its concentration exhibits noticeable spatial variability. Although local fluctuations in the actual flow-rate profiles modify the inhibitor mass-fraction patterns, these variations do not produce meaningful changes in the overall concentration levels along the pipeline. The findings support the design of more effective injection strategies.

Keywords: Core annular flow; flow assurance; multiphase flow; numerical simulation; scale inhibitor.

Affiliated Institution– University of Pernambuco – UPE, Federal University of Pernambuco – UFPE.

Corresponding Author*: Nathália Melo Roseane de Melo*

Affiliated Institution– Petrobras, Federal University of Pernambuco – UFPE.

Corresponding Author*: Deisiane Santos Oliveira*

Affiliated Institution– Federal University of Pernambuco – UFPE.

Corresponding Author*: Anderson Viana do Nascimento, Rebeca Nicolle da Silva, Ellen Raisa Machado de Lima, Fernanda Lira, Paulo Roberto Maciel Lyra, Alessandro Romário Echevarria Antunes, Darlan Karlo Elisiário de Carvalho*

Affiliated Institution– Petrobras.

Corresponding Author*: Giselle Maria Lopes Leite da Silva, Tiago Cavalcante Freitas*

1 INTRODUCTION

Oil and gas production systems frequently operate under multiphase flow conditions in which oil, water, gas, and occasionally solid particles can coexist and interact within the same pipeline. These flows exhibit strong phase coupling, the presence of moving interfaces, and significant spatial variations in physical properties, making their prediction a central challenge in flow assurance engineering [1–4]. In offshore environments, particularly in deepwater and ultra-deepwater fields such as those found in Brazil, the complexity of production systems increases substantially due to long tiebacks, harsh thermodynamic conditions, and the high cost of operational interventions [5–7].

Among the various flow assurance issues encountered in subsea production systems, such as paraffin deposition, hydrate formation, asphaltene precipitation, corrosion, and sand production, inorganic scale deposition stands out as one of the leading causes of well and pipeline blockage [8–10]. Scale formation typically results from changes in pressure, temperature, salinity, or pH as the produced fluid flows through the production system. When the solubility of inorganic salts (e.g., $CaCO_3$, $BaSO_4$, $SrSO_4$) is exceeded, supersaturation, nucleation, agglomeration, and subsequent crystal growth take place, leading to the progressive deposition of mineral layers on internal surfaces [11]. Over time, these deposits reduce the effective flow area, increase pressure losses, impair operational reliability, and may ultimately interrupt production.

Chemical injection of scale inhibitors is one of the most widely adopted mitigation strategies due to its efficiency, relatively low cost, and applicability to a wide range of operational conditions [12, 13]. Many commercial inhibitors are hydrophilic and are injected into the aqueous phase through Chemical Injection Valves (CIVs). Monoethylene glycol (MEG), commonly employed as a hydrate inhibitor and corrosion-mitigation agent, is often used as a solvent for these products [14–16]. However, the effectiveness of these treatments depends strongly on how the injected chemical disperses within the multiphase flow. Incorrect injection rates or unfavorable transport conditions may reduce inhibitor availability in critical regions, enabling the recurrence of scale deposition [9, 17].

Understanding the distribution and transport of scale inhibitors within multiphase and multicomponent flows is therefore essential for designing robust chemical injection strategies. Both experimental studies [18–21] and numerical approaches [22–24] have been employed to investigate behavior under different flow conditions. Recent advances in Computational Fluid Dynamics (CFD) have enabled detailed 3D simulations of multiphase flows using approaches such as the Volume of Fluid (VOF) method [25–27]. These high-fidelity models provide valuable insights into the phase distribution, interfacial behavior, and species transport that cannot be captured by 1D mechanistic models or empirical correlations. In oil pipelines operating under annular oil-water flow regimes [28], common in deepwater risers, the aqueous phase travels near the pipe wall, and therefore governs the transport of hydrophilic inhibitors. For this reason, analyzing the coupling between multiphase hydrodynamics and species dispersion is critical for understanding inhibitor concentration profiles along the line [29, 30].

Combined 1D–3D workflows further enhance predictive capability in chemical-injection studies. 1D transient multiphase flow simulators, such as ALFAsim [31], LedaFlow [32] and OLGA [33], efficiently capture the global hydrodynamic and thermodynamic conditions along long offshore pipelines, including pressure profiles, temperature gradients, and flow-pattern evolution. These large-scale predictions provide the boundary and operating conditions required to initialize high-fidelity 3D CFD models. In turn, 3D simulations resolve the local mixing processes, interfacial dynamics, and species-transport mechanisms in the immediate vicinity of the injection point. This integrated approach has been increasingly adopted in recent flow-assurance investigations. Rosa et al. [34], for example, evaluated chemical-injection strategies for wax-control in unconventional wells, emphasizing the importance of accurately capturing local dispersion and phase interactions to ensure adequate inhibitor availability throughout the system.

Integrated 1D–3D methodologies have been applied to problems such as slug hydrodynamics, wax

transport, and chemical-injection optimization under offshore conditions [35–38]. Although these studies demonstrate the value of coupling system-scale and near-field simulations, most existing investigations remain centered on thermal–hydraulic behavior or on wax-mitigation chemistry. In oil-water flows operating in annular or core-annular regimes, the transport of hydrophilic scale inhibitors depends strongly on the local distribution of the aqueous phase. Yet, detailed analyses addressing scaling mitigation through chemical injection in such flow patterns are scarce [11, 39, 40]. This gap motivates the development of coupled 1D–3D numerical frameworks capable of quantifying local dispersion mechanisms and improving the design of chemical-injection strategies for scale control in offshore production pipelines.

In this context, the present work investigates the dispersion of a scale inhibitor (MEG-based solution) injected into an oil-production pipeline operating under oil–water annular two-phase flow. The study integrates 1D simulations (ALFAsim) to establish global operating conditions and high-resolution 3D CFD simulations (ANSYS Fluent [41]) to characterize local multiphase and multicomponent flow behavior near the injection point. Four injection scenarios are analyzed, each defined by nominal injection rates specified by the valve manufacturer and their corresponding real measured values. The objective is to evaluate how flow regimes, phase distribution, and injection rates affect the transport and mixing of the inhibitor.

The results provide insights into the spatial distribution of inhibitor concentration, highlighting the confinement of the chemical within the aqueous phase and its progressive homogenization along the pipe length. These findings contribute to improving chemical-injection practices and supporting the design of more effective flow-assurance strategies in offshore oil production systems.

2 METHODOLOGY

This work employs an integrated 1D–3D numerical framework to evaluate the dispersion of a scale inhibitor injected into an oil–water core-annular flow representative of deepwater production conditions. The methodology combines a one-dimensional simulator, used to compute system-scale operational profiles along the entire pipeline, and a high-fidelity 3D CFD simulator, used to resolve near-field mixing, species transport, and inhibitor distribution in the vicinity of the Chemical Injection Valve (CIV). All simulations were carried out using ALFAsim [31] and ANSYS Fluent [41]. The combined use of the two software programs is outlined in Fig. 1.

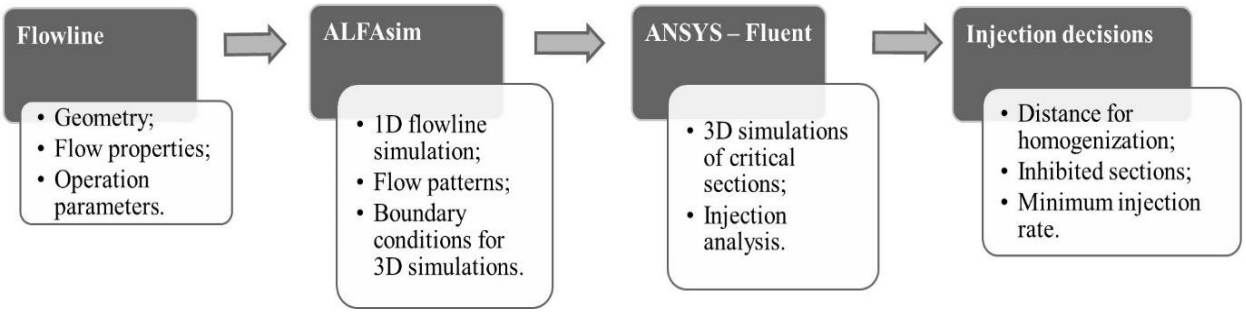

Figure 1: Methodology outline for simulation.

In the cases examined in this study, the inhibitor formulation contains less than 10% (by mass) of the active component, while the remaining fraction is predominantly monoethylene glycol (MEG), which acts as the solvent. Since the numerical simulations focus on the hydrodynamic behavior and transport of the injected fluid along the pipeline (rather than chemical reactions), the physical and thermodynamic properties of pure MEG were assumed to represent those of the injected inhibitor solution. This assumption provides a simplified yet adequate approach for modeling purposes.

2.1 1D MODEL (ALFASIM)

The 1D simulations were carried out using the commercial multiphase-flow simulator ALFAsim (version 2024.3.1) [31]. In this step, the production line is modeled with a multi-field formulation (Multi-Field Model), in which each physical phase may be represented by a continuous and a dispersed field [42, 43]. For each field k, the mass conservation equation can be written as

$$\frac{\partial(\alpha_k\rho_k)}{\partial t}+\frac{\partial(\alpha_k\rho_k u_k)}{\partial x}=\sum_{s=1}^{N_{\text{sources}}}\Gamma_{k,s} \tag{1}$$

where α_k is the volume fraction, ρ_k the density, u_k the axial velocity of field k, and $\Gamma_{k,s}$ denotes the mass source term.

The corresponding momentum balance for field k is expressed as

$$\begin{aligned}\frac{\partial(\alpha_k\rho_k u_k)}{\partial t}+\frac{\partial(C_k\alpha_k\rho_k u_k^2)}{\partial x}&=-\alpha_k\frac{\partial p_k}{\partial x}+\alpha_k\rho_k g\sin\theta+(p_{ki}-p_k)\frac{\partial\alpha_k}{\partial x}\\&+\frac{\tau_{wk}S_{wk}}{A}+\frac{\tau_i S_i}{A}\pm F_k^{vm}+F_k^{drag}+\sum_{s=1}^{N_{\text{sources}}}\Gamma_{k,s}\,\bar{u}_{k,s}\end{aligned} \tag{2}$$

where θ is the inclination angle, A is the cross-sectional area, p_k is the field pressure, p_{ki} is the interfacial pressure, τ_{wk} and τ_i are wall and interfacial shear stresses, S_{wk} and S_i are wetted perimeters, C_k is the velocity-distribution parameter, and F_k^{vm} and F_k^{drag} represent additional volumetric and drag forces.

For the energy balance, a global mixture equation is adopted:

$$\begin{aligned}&\frac{\partial}{\partial t}\left(\sum_k\alpha_k\rho_k\left[h_k+\frac{u_k^2}{2}\right]\right)+\frac{\partial}{\partial x}\left(\sum_k\alpha_k\rho_k u_k\left[h_k+\frac{u_k^2}{2}\right]\right)\\&=\frac{\partial p}{\partial t}+\sum_k\alpha_k\rho_k u_k g\sin\theta+\dot{Q}_{\text{source}}+\dot{Q}_{\text{wall}}\end{aligned} \tag{3}$$

2.2 3D MODEL (ANSYS FLUENT)

The 3D simulations were conducted in transient regime using ANSYS Fluent 2024 R1 [41], considering a turbulent, incompressible, non-isothermal, and multicomponent two-phase flow representative of offshore oil production.

The Eulerian Volume of Fluid (VOF) method [25] was employed to capture the interface between immiscible liquids. The phase volume fraction α_k satisfies:

$$\frac{1}{\rho}\left[\frac{\partial}{\partial t}(\alpha_k\rho_k)+\nabla\cdot(\alpha_k\rho_k\vec{v}_k)\right]=S_{\alpha_k}+\sum_{q=1}^{n}(\dot{m}_{qk}-\dot{m}_{kq}) \tag{4}$$

where ρ is the mixture density and $\vec{v}_k$ is the phase velocity.

The mixture momentum equation is

$$\begin{aligned}\frac{\partial}{\partial t}(\rho\vec{v})+\nabla\cdot(\rho\vec{v}\vec{v})&=-\nabla p+\nabla\cdot\left[\mu(\nabla\vec{v}+\nabla\vec{v}^T)-\frac{2}{3}(\nabla\cdot\vec{v})I\right]\\&+\rho\vec{g}+\vec{F}\end{aligned} \tag{5}$$

where $\vec{F}$ includes surface-tension effects.

Energy conservation is written as

$$\frac{\partial}{\partial t}(\rho E)+\nabla\cdot[\vec{v}(\rho E+p)]=\nabla\cdot\left(k_{\text{eff}}\nabla T-\sum_k\sum_j h_{j,k}\vec{J}_{j,k}+\bar{\tau}_{\text{eff}}\vec{v}\right)+S_h \tag{6}$$

Surface tension was modeled by the CSF approach [44]:

$$F_{\text{vol}}=\sum_{q<k}\sigma_{qk}\frac{\alpha_q\rho_q\kappa_k\nabla\alpha_k+\alpha_k\rho_k\kappa_q\nabla\alpha_q}{0.5(\rho_q+\rho_k)} \tag{7}$$

The VOF formulation was solved implicitly. Interface reconstruction was performed using a second-order compressive scheme to preserve interface sharpness and reduce numerical diffusion along the phase boundary.

Species transport was modeled using the non-reacting multicomponent formulation [41]:

$$\begin{aligned}&\frac{\partial}{\partial t}\left(\rho_k\alpha_k Y_{i_k}\right)+\nabla\cdot\left(\rho_k\alpha_k\vec{v}_k Y_{i_k}\right)=-\nabla\cdot\left(\alpha_k\vec{J}_{i_k}\right)+\alpha_k R_{i_k}+\alpha_k S_{i_k}+\\&\sum_{q=1}^{n}\dot{m}_{q^i k^j}+R\end{aligned} \tag{8}$$

with diffusive flux

$$\vec{J}_{i,k}=-\left(\rho D_{i_{k,m}}+\frac{\mu_t}{Sc_t}\right)\nabla Y_{i_k}-D_{T,i_k}\frac{\nabla T}{T} \tag{9}$$

Turbulence closure was provided by the standard k-ε RANS model [45] with enhanced wall treatment [46,47].

2.3 NUMERICAL STRATEGIES

The 1D simulation was performed in steady state using ALFAsim's default numerical settings. The 3D simulations used a pressure-based solver with SIMPLEC [48] for pressure–velocity coupling. Gradients were computed using the Least Squares Cell-Based method. Pressure interpolation used PRESTO! [41]. Momentum, turbulence variables, energy, and species transport employed Second-Order Upwind discretization. The volume fraction equation used a compressive scheme. The transient formulation was implicit.

Convergence per time step was monitored by absolute residuals, requiring 10^{-3} for mass, momentum, turbulence variables, volume fraction, and species; and 10^{-6} for energy, or a maximum of 10 iterations per time step [41].

The time step Δt followed the stability criteria proposed by [49], combining advective and diffusive limits. A grid-convergence study using the Grid Convergence Index (GCI) was conducted following [50,51].

For initialization, turbulence quantities were estimated as [52,53]

$$k = \frac{3}{2}(UI)^2 \tag{10}$$

$$\varepsilon = C_\mu^{3/4} \frac{k^{3/2}}{L} \tag{11}$$

with $C_\mu = 0.09$.

A control-volume region corresponding to the expected oil core was used to generate a pathline-based initialization to ensure a fully developed annular pattern at the beginning of the transient simulation.

2.4 DESCRIPTION OF THE CASES

The analyzed production line includes a well and riser, as shown in Fig. 2. The CIV is located at a height of 277.7 m from the start of the well. The well is vertical with a length of 3,539 m, while the riser has a vertical projection of 2,015 m and a horizontal projection of 5,000 m, resulting in a total line length of 9,956.8 m. The internal pipe diameter is 4.7 in. The inhibitor inlet diameter is 1.01×10^{-2} m, corresponding to the CIV orifice installed in the Chemical Injection Mandrel (CIM).

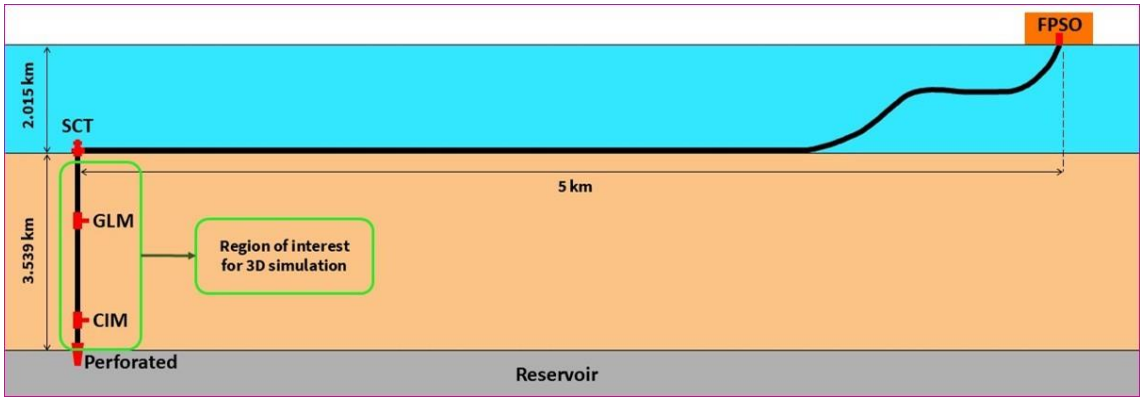

Figure 2: Flow line.

The production system is divided into two main sections: (i) the well, extending from the perforated region through the CIM and the Gas-Lift Mandrel (GLM) up to the Subsea Christmas Tree (SCT); and (ii) the riser, spanning from the SCT to the Floating Production Storage and Offloading unit (FPSO), as illustrated in Fig. 2.

The entire production line is represented in the 1D model. A uniform pipe roughness of 4.57×10^{-5} m is considered. The operating scenario corresponds to an oil flow rate of $1{,}146.6\ \mathrm{m^3/d}$, a

water flow rate of 770.33 sm^3/d, and a gas–oil ratio at the bubble point of 243. Under standard conditions, the oil and water densities are set to 891.67 kg/m³ and 1,001 kg/m³ respectively. The 1D simulation is performed in steady state to provide boundary/initial conditions for the 3D analysis.

The 3D CFD domain corresponds to a representative 45.3 m section downstream of the CIV, where the aqueous phase occupies the wall region and the oil phase flows in the core (Fig. 3).

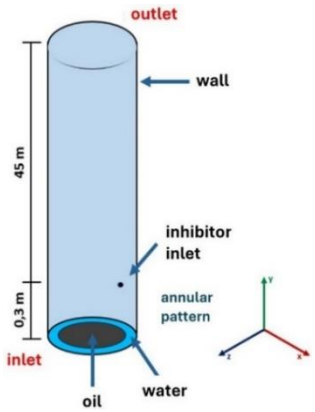

Figure 3: Schematic profile (not to scale) of the pipeline section analyzed.

To ensure consistency between global and local models, inlet pressure, flow rate, phase fractions, flow patterns, and fluid properties were obtained from the ALFAsim solution. The inhibitor enters through the CIV orifice, with prescribed species mass fraction at the injection inlet.

Twelve simulations were performed, corresponding to four opening percentages of two GIC models, identified in this study as V1 and V2. For each opening, three injection conditions were evaluated: (i) the nominal dosage rate specified by the manufacturer and (ii) two actual operating rates obtained from field measurements for each of the GICs considered.

The nominal and real injection flow rates were grouped into four cases (Figs. 4–7):

- Case 1 – Nominal flow rate 01 (2 L/h): 6.18×10^{-4} kg/s, and real flow rates:

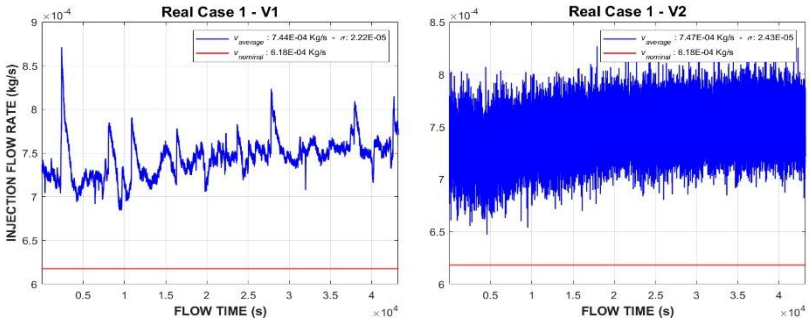

Figure 4: Case 1 – Real flow rates.

- Case 2 – Nominal flow rate 02 (5 L/h): 1.54×10^{-3} kg/s, and real flow rates:

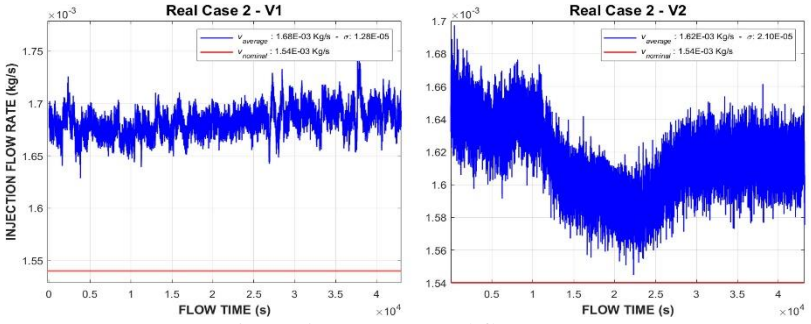

Figure 5: Case 2 – Real flow rates.

- Case 3 – Nominal flow rate 03 (10 L/h): 3.09×10^{-3} kg/s, and real flow rates:

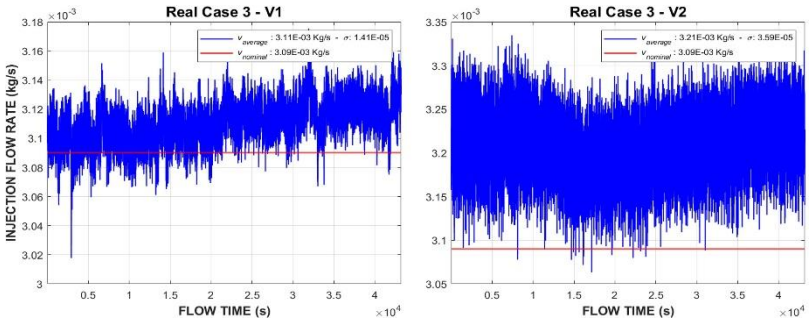

Figure 6: Case 3 – Real flow rates.

- Case 4 – Nominal flow rate 04 (24 L/h): 7.42×10^{-3} kg/s, and real flow rates:

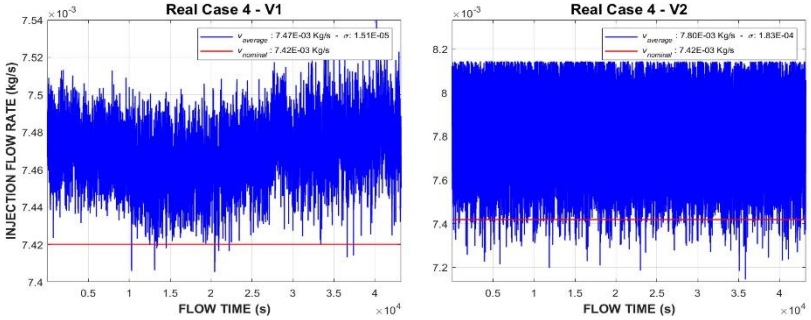

Figure 7: Case 4 – Real flow rates.

In all cases, the inhibitor was injected for 50 s of physical time, which was sufficient for the hydrodynamic and species fields to reach quasi-steady behavior at the monitored cross-sections. Therefore, the valve flow-rate plots were limited to 50 s.

Table 1 presents the thermophysical properties used in the 3D simulations.

Table 1: Thermophysical properties of the inhibitor, crude oil, formation water, and steel.

Property	Inhibitor	Oil	Water	Steel
Density $[kg/m^3]$	1111.4	872.253	992.858	8030
Specific heat $[J/(kg \cdot K)]$	2415	1932.53	4173.81	502.48
Thermal conductivity $[W/(m \cdot K)]$	0.252	0.14055	0.631025	16.27
Viscosity $[kg/(m \cdot s)]$	0.0157	0.00915495	0.00064096	–
Molecular weight $[g/mol]$	62.0482	189.86	18.0152	–
Standard-state enthalpy $[J/kgmol]$	0	75778.2	–245186	–
Reference temperature $[K]$	298.15	353.15	353.15	–

Gravitational acceleration was set to $g = 9.81\ m/s^2$ in the y-direction. Operating pressure settings followed the fully submerged pipeline condition: the manometric outlet pressure (39.14 MPa) was defined as the operating pressure, and boundary pressures were specified relative to this value. Turbulence quantities at the oil and water inlets used the empirical turbulence intensity correlation [41]:

$$I = 0.16\,\mathrm{Re}^{-1/8} \tag{12}$$

Water and oil Reynolds numbers were estimated as $\mathrm{Re}_w \approx 162{,}833$ and $\mathrm{Re}_o \approx 22{,}274$ [54]. A turbulence intensity of 2% was prescribed for the inhibitor inlet; 5% was used at the outlet.

3 RESULTS AND DISCUSSION

3.1 1D SIMULATION RESULTS

This section presents the results obtained from the 1D simulations, which were performed to characterize the global hydrodynamic behavior of the production system and to provide boundary conditions for the 3D analyses. The Figure 8 are presented shows the pressure and temperature profiles, as well as flow patterns, obtained in the well.

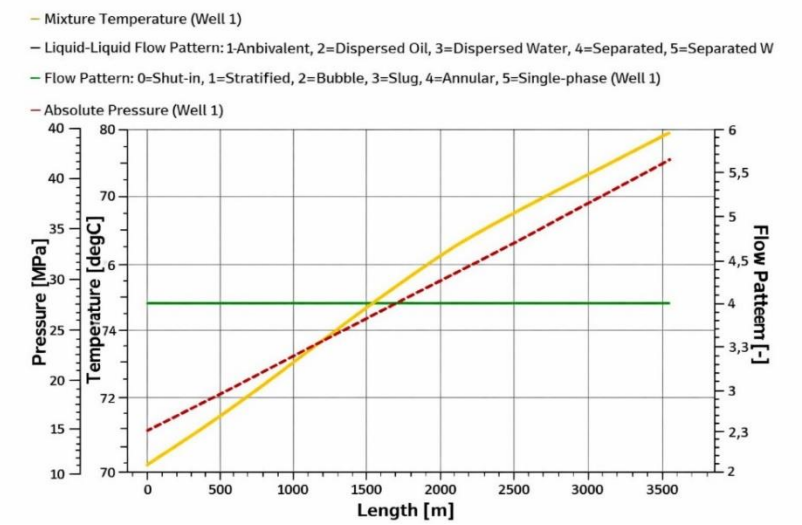

Figure 8: 1D simulation results in the well.

The Figure 9 are presented shows the pressure and temperature profiles, as well as flow patterns, obtained in the riser.

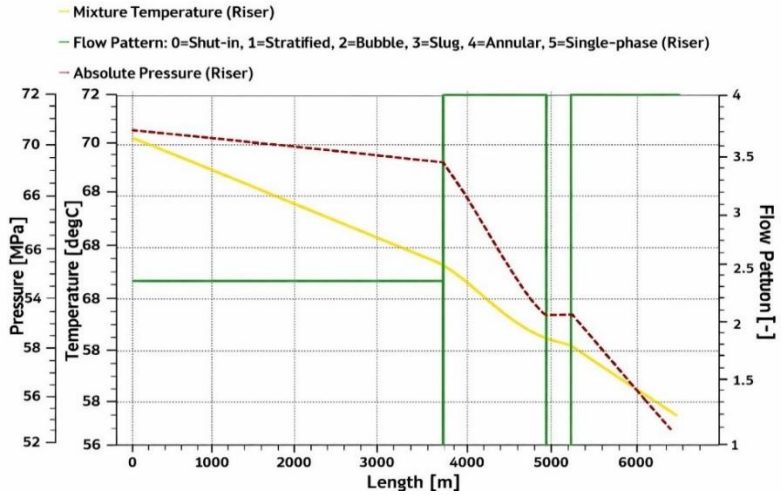

Figure 9: 1D simulation results in the riser.

These results were used to obtain the boundary conditions presented in Sec. 3.
As shown in Fig. 8, the flow pattern is annular throughout the well. In the riser (Fig. 9), due to the presence of horizontal and inclined sections, the flow pattern alternates between annular and stratified.

3.2 GRID-CONVERGENCE STUDY

A grid-convergence study was carried out using the Grid Convergence Index (GCI) methodology. Using the nominal flow rate 01 (2 L/h), the maximum, minimum, and mean values of the inhibitor mass fraction, expressed in parts per million (ppm), obtained for three meshes are shown in Fig. 10. The coarse mesh (Mesh 03) contains 3,094,668 cells, the

medium mesh (Mesh 02) contains 6,884,782 cells, and the fine mesh (Mesh 01) contains 15,891,100 cells.

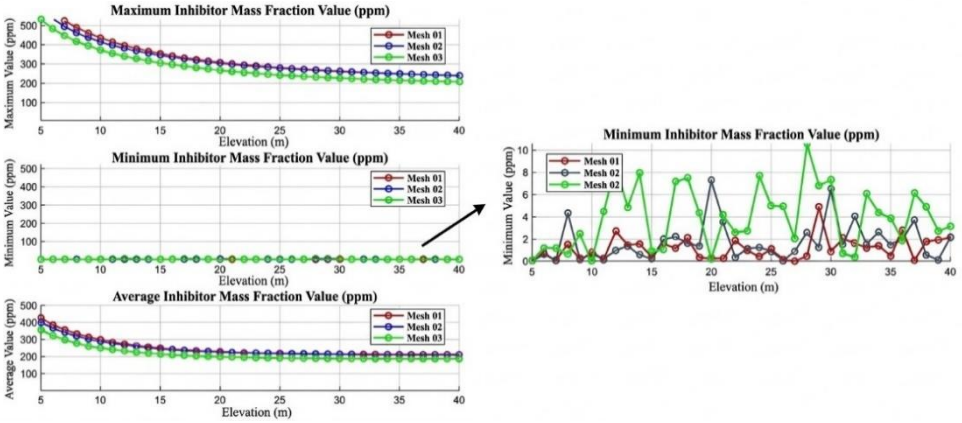

Figure 10: Inhibitor mass fraction results for the three meshes used in the convergence study.

Figure 10 indicates that the maximum and mean inhibitor mass fraction values predicted using Mesh 02 are very close to those obtained with Mesh 01. For some cross-sections, identical values were obtained, suggesting mesh-independent behavior for the variable of interest.

Table 2 summarizes the main parameters and results of the GCI analysis [50].

Table 2: Grid Convergence Index (GCI) parameters and results.

Parameter	Value	Description
N_1	15,891,100	Number of cells (fine mesh)
N_2	6,884,782	Number of cells (medium mesh)
N_3	3,094,668	Number of cells (coarse mesh)
r_{12}	1.3216	Refinement ratio (medium → fine)
r_{23}	1.3054	Refinement ratio (coarse → medium)
$t_{\text{sim},1}$	132h 05min	Simulation time (fine mesh)
$t_{\text{sim},2}$	62h 29min	Simulation time (medium mesh)
$t_{\text{sim},3}$	26h 49min	Simulation time (coarse mesh)
ϕ_1	3.0×10^{-4}	Numerical solution (fine mesh)
ϕ_2	1.0×10^{-4}	Numerical solution (medium mesh)
ϕ_3	3.0×10^{-4}	Numerical solution (coarse mesh)
p	3.9286	Apparent order of accuracy
ϕ_{ext}	3.0×10^{-4}	Richardson extrapolated solution
e_a^{12}	4.2504	Approx. relative error (medium → fine)
e_a^{23} (%)	4.2504	Approx. relative error (coarse → medium)
e_{ext}^{12} (%)	6.2526	Extrapolated rel. error (medium → fine)
e_{ext}^{23}(%)	6.2526	Extrapolated rel. error (coarse → medium)
GCI_{12} (%)	2.6696	GCI (fine mesh)
GCI_{23}(%)	8.3370	GCI (medium mesh)
AR	0.9575	Asymptotic range indicator ($AR \approx 1$)

The results indicate that Mesh 02 satisfies the grid-convergence requirements. GCI_{12} = 2.67% indicates a small difference between the two most refined meshes, while GCI_{23} = 8.34% shows a larger discrepancy between coarse and medium meshes. AR is close to unity, supporting asymptotic convergence. Mesh 02 was selected for subsequent simulations due to its accuracy and reduced computational cost.

3.3 CASE ANALYSIS

The 3D simulations were grouped into four analysis cases, each corresponding to a nominal injection rate specified by the valve manufacturer and two associated real field-measured injection rates, totaling twelve simulations under fully developed core-annular flow. The discussion focuses on the flow field and inhibitor dispersion behavior at t = 50 s, when the monitored variables exhibited stable qualitative and quantitative responses.

The Figure 11 presents a detailed visualization of the inhibitor mass fraction color maps in different cross-sections of the pipe in Case 1. In the figure, complete standardization of the color scales would significantly impair the visualization of regions with low MEG concentration. Therefore, individual scales were adopted in order to preserve the physical interpretation of the concentration gradients.

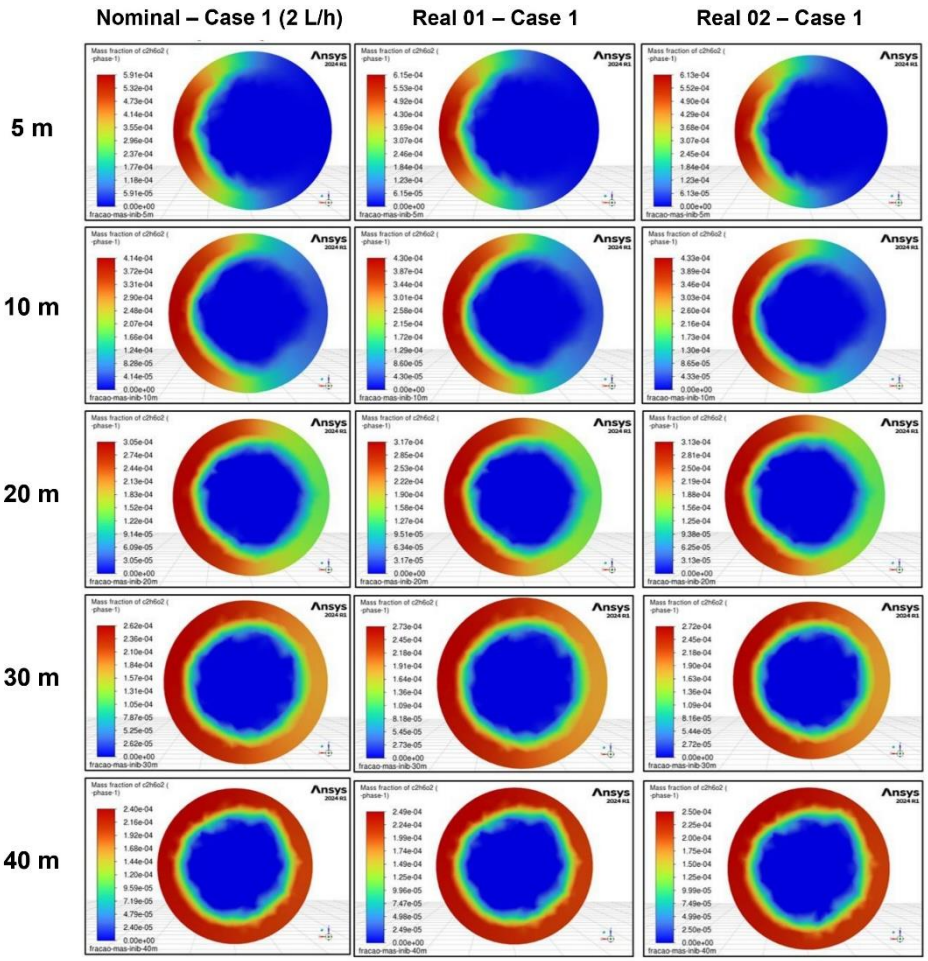

Figure 11: Distribution of the MEG mass fraction for Case 1 under the Nominal, Real 01, and Real 02 flow rate conditions at different axial positions along the pipeline.

Figure 12 shows the longitudinal evolution of the maximum, minimum, and average values of the inhibitor mass fraction in Case 1.

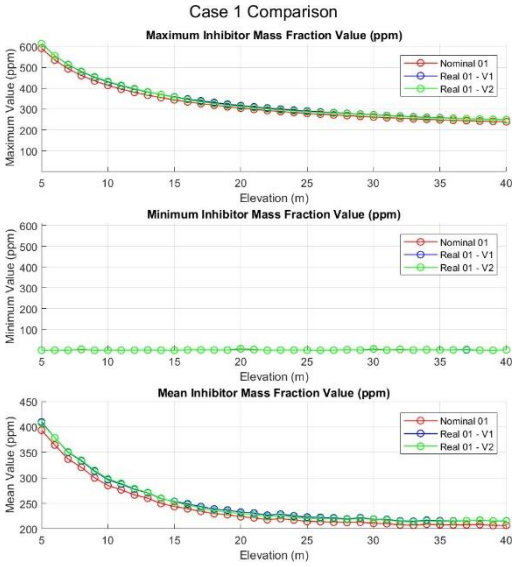

Figure 12: Inhibitor mass fraction results for Case 1.

The inhibitor remains confined to the aqueous annular layer, with higher concentrations near

the CIV and a locally heterogeneous distribution in the near-injection region. This behavior is associated with strong advective transport in the continuous water film and shear interaction with the oil core. Along the pipeline elevation, the concentration field becomes progressively more uniform, indicating the combined action of turbulent dispersion and stabilization of the annular regime.

For the remaining cases (Cases 2–4), the analysis is presented in terms of maximum, minimum, and mean inhibitor mass fraction along the pipeline height. Figure 13 shows the longitudinal evolution of the maximum, minimum, and average values of the inhibitor mass fraction in Case 2.

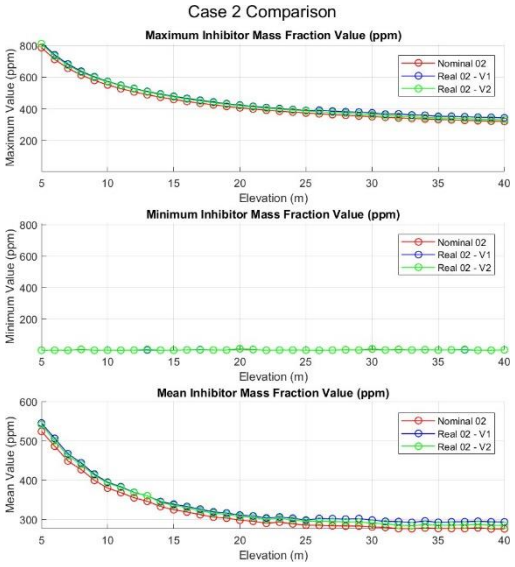

Figure 13: Inhibitor mass fraction results for Case 2.

Figure 14 shows the longitudinal evolution of the maximum, minimum, and average values of the inhibitor mass fraction in Case 3.

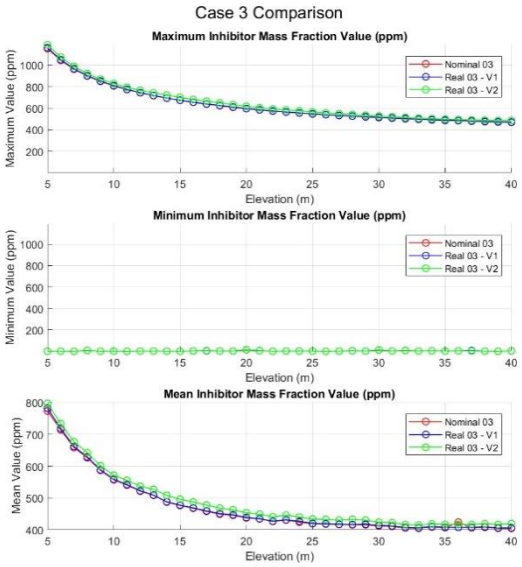

Figure 14: Inhibitor mass fraction results for Case 3.

Figure 15 shows the longitudinal evolution of the maximum, minimum, and average values of the inhibitor mass fraction in Case 4.

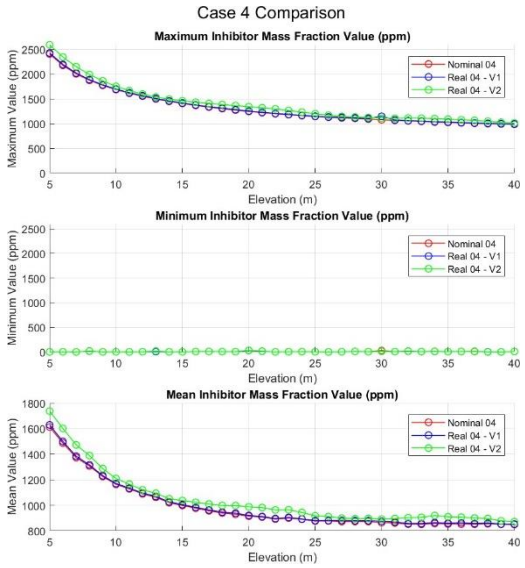

Figure 15: Inhibitor mass fraction results for Case 4.

In these cases, the numerical simulations carried out made it possible to observe that global trends are consistent with Case 1. The inhibitor is transported within the aqueous annulus, peaks near the CIV, and tends toward homogenization from approximately 30 m above the injection point as the flow stabilizes.

Comparisons between nominal and real injection rates within each case show only small deviations of the same order of magnitude, without changes in the qualitative dispersion pattern. Moderate fluctuations in injected flow rate do not significantly affect inhibitor distribution along the aqueous annulus, indicating robustness under realistic operational variability.

The stabilized mean inhibitor concentration (ppm) at each monitored cross-section increases proportionally with injection rate, indicating a direct relationship between these variables. In Case 1 (210 ppm nominal), stabilized mean values were 217 ppm (V1) and 208 ppm (V2). In Case 2 (280 ppm nominal), means were 295 ppm (V1) and 288 ppm (V2). In Case 3 (408 ppm nominal), means were 410 ppm (V1) and 421 ppm (V2). In Case 4 (854 ppm nominal), stabilized means reached 864 ppm (V1) and 881 ppm (V2). Overall, both valves yielded comparable dispersion outcomes; V2 tended to slightly higher mean ppm at the highest injection rates, while V1 showed closer agreement with nominal values at intermediate cases.

4 CONCLUSION

This study proposes an integrated numerical strategy combining one-dimensional (1D) and three-dimensional (3D) simulations to investigate the injection and transport of a scale inhibitor in an offshore oil-production pipeline operating under core-annular flow conditions. The 1D simulations performed in ALFAsim provided global pressure and temperature profiles, as well as the prevailing flow pattern along the production line, allowing an efficient characterization of the large-scale operating conditions. These results were used to define consistent boundary conditions for the 3D CFD simulations carried out in ANSYS Fluent, enabling a detailed evaluation of the local hydrodynamics and the spatial distribution of the injected inhibitor in the region of greatest operational interest.

The 3D results showed that the inhibitor remains confined to the aqueous annular layer for all injection rates evaluated, indicating that the continuous water phase acts as an

effective carrier. Advective transport was dominant, while molecular diffusion played a minor role and turbulent dispersion contributed to the radial and axial spreading of the inhibitor within the annular film. In the upstream portion of the domain, the concentration field exhibited local heterogeneity due to strong advection; however, from approximately 30 m above the injection point, the concentration became progressively more uniform as the core-annular flow stabilized and turbulent mixing became more effective.

The comparison between nominal and measured injection conditions revealed very similar inhibitor mass-fraction distributions, with only small deviations of the same order of magnitude. This indicates low sensitivity of dispersion to moderate injection-rate fluctuations, supporting robustness of the chemical-injection system under typical operational variability. From an applied perspective, the results provide guidance for flow-assurance planning and injection strategies, indicating that minor operational oscillations do not significantly compromise inhibitor delivery along the pipeline.

Future developments will extend the framework by (i) simulating longer pipeline segments, (ii) evaluating additional flow patterns and operating conditions, (iii) applying machine-learning techniques to build predictive surrogate models from CFD datasets, (iv) incorporating inorganic scale formation models at the wall to assess inhibitor performance under reactive conditions, and (v) analyzing additional flow-assurance scenarios.

5 ACKNOWLEDGMENTS

This research was supported by Petrobras (project number 2023/00049-1), FACEPE (IBPG-0009-3.01/21), and CNPq (process numbers PQ-308334/2019-1 and PQ-310145/2021-0). The authors also acknowledge Petrobras for providing field data and technical support.

6 REFERENCES

[1] Ishii M, Hibiki T. Thermo-Fluid Dynamics of Two-Phase Flow. 2nd ed. New York: Springer; 2011.

[2] Crowe CT, Schwarzkopf JD, Sommerfeld M, Tsuji Y. Multiphase Flows with Droplets and Particles. 2nd ed. Boca Raton: CRC Press; 2011. doi:10.1201/b11103.

[3] Yadigaroglu G, Hewitt GF. Introduction to Multiphase Flow: Basic Concepts, Applications and Modelling. Cham: Springer; 2018. doi:10.1007/978-3-319-58718-9.

[4] Habibi A, Fensky CE, Roostaei M, Mahmoudi M, Fattahpour V, Zeng H, et al. A laboratory workflow for characterization of scaling deposits in thermal wells. Energies. 2020;13(12):3184. doi:10.3390/en13123184.

[5] Pedroso CA, Silva GR, Range P, Nunes KR. Subsea systems innovations and the use of state of art subsea technologies help the flow assurance of heavy oil production in ultra-deep waters. In: Rio Oil & Gas Expo and Conference 2020; 2020 Dec 1–3; Rio de Janeiro, Brazil. Rio de Janeiro: Instituto Brasileiro de Petróleo e Gás; 2020. p. 1-20.

[6] Camargo RMT, Gonçalves ML, Montesanti JRT, et al. A perspective view of flow assurance in deepwater fields in Brazil. SPE International Conference on Health, Safety, and Environment in Oil and Gas Exploration and Production. 2004 May. doi:10.4043/16687-MS.

[7] L. das D. Cardoso. Proposta de método e sistema para otimizar o controle da

taxa de corrosão em tubulações da indústria petrolífera [PhD thesis]. Rio de Janeiro: North Fluminense State University Darcy Ribeiro; 2020.

[8] Granbakken D, Haarberg T, Rollheim M, Østvold T, Read P, Schmidt T. Scale formation in reservoir and production equipment during oil recovery. III. A kinetic model for the precipitation/dissolution reactions. Acta Chem Scand. 1991;45:892-901.

[9] Al Rawahi Y. M, Shaik F. Studies on scale deposition in oil industries & their control. International Journal for Innovative Research in Science & Technology (IJIRST), 2017;12(3):152-167.

[10] Brandão RC, Gomes MF, Ferreira LF, Guimarães RG, Moriconi L, Loureiro JBR. Investigação experimental da influência da temperatura no fenômeno de incrustação de carbonato de cálcio formado em um escoamento interno a alto Reynolds. In: Encontro Nacional de Construção de Poços de Petróleo e Gás (ENAHPE); 2023 Aug; Brazil. p. 1-7.

[11] Kumar A. Perspectives of flow assurance problems in oil and gas production: a mini-review. Energy Fuels. 2023;37(12):8142-8159. doi:10.1021/acs.energyfuels.3c00843.

[12] Graham GM, Mackay EJ, Dyer SJ, Bourne HM. The challenges for scale control in deepwater production systems: chemical inhibition and placement. In: Proceedings of CORROSION 2002; 2002 Apr 7-12; Denver, CO, USA. Houston: AMPP; 2002. p. 1-36. doi:10.5006/C2002-02316.

[13] Kamal MS, Hussein I, Mahmoud M, Sultan AS, Saad MAS. Oilfield scale formation and chemical removal: a review. Journal of Petroleum Science and Engineering. 2018;171:127-139. doi:10.1016/j.petrol.2018.07.037.

[14] Solano SDM. Experimental and computational investigation on the displacement and mixing mechanisms in well-head jumpers during restart with monoethylene glycol [master's thesis]. Tulsa (OK): The Graduate School, The University of Tulsa; 2010.

[15] Volk M. Displacement & mixing in subsea jumpers: experimental data & CFD simulations. Tulsa (OK): Research Partnership to Secure Energy for America (RPSEA); 2013.

[16] Widyanto B, Wiguna IGBAES. The effect of mono ethylene glycol on the top of line corrosion rate of low carbon steel in acetic acid and elevated temperature environment. Heliyon. 2019;5(8):e02006. doi:10.1016/j.heliyon.2019.e02006.

[17] Olajire AA. A review of oilfield scale management technology for oil and gas production. Journal of Petroleum Science and Engineering. 2015;135:723-737. doi:10.1016/j.petrol.2015.09.011.

[18] Kiaei Z, Haghtalab A. Experimental study of using Ca-DTPMP nanoparticles in inhibition of CaCO3 scaling in a bulk water process. Desalination. 2014;338:84-92. doi:10.1016/j.desal.2014.01.027.

[19] Sanni OS, Bukuaghangin O, Charpentier TVJ, Neville A. Evaluation of laboratory techniques for assessing scale inhibition efficiency. Journal of Petroleum Science and Engineering. 2019;182:106347. doi:10.1016/j.petrol.2019.106347.

[20] Peng D, Wu Y, Tan Z, Wu S, Chen Y, Liu J. Experimental study on scale inhibition performance and fouling characteristics of spiral insert in heat transfer tube. Thermal Science and Engineering Progress. 2024;50:102567. doi:10.1016/j.tsep.2024.102567.

[21] Gao WL, Sun LW, Li M, Ye XA, Gao QC, Kong DL, et al. Synthesis and performance evaluation of modified polyaspartic-acid-based scale inhibitor. Energies. 2024;17(13):3195. doi:10.3390/en17133195.

[22] Mackay EJ, Matharu AP, Sorbie KS, Jordan MM, Richard T. Modeling scale-inhibitor treatments in horizontal wells: application to the Alba field. SPE Production & Facilities. 2000;15:107-114. doi:10.2118/63013-PA.

[23] Beteta A, Vazquez O, Al Kalbani MM, Eze F. Simulation of scale inhibitor squeeze treatments in a polymer flooded reservoir. In: SPE International Conference on Oilfield Chemistry; 2021 Dec; The Woodlands, TX, USA. doi:10.2118/204367-MS.

[24] Kalantari Meybodi M, Sorbie KS, Vazquez O, Mackay E. Coupled adsorption/precipitation (Γ/Π) modelling of scale inhibitor transport in porous media using the coupled isotherm, AΓΠ(c). Colloids and Surfaces A: Physicochemical and Engineering Aspects. 2024;703:135309. doi:10.1016/j.colsurfa.2024.135309.

[25] Hirt CW, Nichols BD. Volume of fluid (VOF) method for the dynamics of free boundaries. Journal of Computational Physics. 1981;39(1):201-225. doi:10.1016/0021-9991(81)90145-5.

[26] Abdullameer L, Rashid FL, Hussein EQ, Al-Obaidi MA, Abbas SJ. Simulation and analysis of multiphase flow in pipelines utilising ANSYS Fluent. In: ICSET 2024: 5th International Conference for Sustainable Engineering Techniques; 2024; Baghdad, Iraq. doi:10.2478/9788368412031-006.

[27] Jadidi SA, Anbalagan S, Moolya S. Numerical analysis of heavy oil-water-air flow in a horizontal pipe using core annular flow adapting large eddy simulations. Energies. 2025;18(23):6188. doi:10.3390/en18236188.

[28] Xie B, Jiang F, Lin H, Zhang M, Gui Z, Xiang J. Review of core annular flow. Energies. 2023;16(3):1496. doi:10.3390/en16031496.

[29] Ruiz-Díaz CM, Quispe-Suarez B, González-Estrada OA. Two-phase oil and water flow pattern identification in vertical pipes applying long short-term memory networks. Emergent Materials. 2024. doi:10.1007/s42247-024-00631-2.

[30] Nascimento JCS. Simulador de escoamento multifásico em poços de petróleo (SEMPP) [master's thesis]. Natal: Federal University of Rio Grande do Norte; 2013.

[31] ESSS. ALFAsim artificial lift and flow assurance simulator technical manual. Rev ed. Florianópolis: ESSS; [date unknown].

[32] Danielson TJ, Bansal KM, Djoric B, Duret E, Johansen ST, Hellan Ø. Testing and qualification of a new multiphase flow simulator. In: Offshore Technology Conference; 2011 May; Houston, TX, USA. doi:10.4043/21417-MS.

[33] Bendiksen KH, Malnes D, Moe R, Nuland S. The dynamic two-fluid model OLGA:

theory and application. SPE Production Engineering. 1991;6(2):171-180. doi:10.2118/19451-PA.

[34] Rosa RMD, Soprana AB, Girardi V, Villagra FM. Assessment of chemical injection to mitigate wax deposition in unconventional wells. In: SPE Annual Technical Conference and Exhibition; 2021 Sep; Dubai, UAE. doi:10.2118/206206-MS.

[35] Xing L, Yeung H, Geng Y, Cao Y, Shen J. Study on hydrodynamic slug flow mitigation with wavy pipe using a 3D–1D coupling approach. Computers & Fluids. 2014;99:104-115. doi:10.1016/j.compfluid.2014.04.023.

[36] Johansen ST, Mo S, Meese E, Oliveira JES, Reyes JFR, Carneiro JNE. CFD simulations of multiphase flows containing large scale interfaces and dispersed phases with selected production technology applications. In: OTC Brasil; 2015 Oct; Rio de Janeiro, Brazil. doi:10.4043/26303-MS.

[37] Prado Rojas JE, Goedert F, Barbosa Neto AM, Alves MVC. Isothermal and non-isothermal multiphase flow steady-state simulation of offshore production systems using ALFAsim. International Journal of Oil, Gas and Coal Technology. 2022;30(4):335-358. doi:10.1504/IJOGCT.2022.124419.

[38] Xu B, Zhang K. GPSFlow/Hydrate: a new numerical simulator for modeling subsurface multicomponent and multiphase flow behavior of hydrate-bearing geologic systems. Journal of Marine Science and Engineering. 2025;13:1622. doi:10.3390/jmse13091622.

[39] Rodriguez-Hernandez CD, Chen T, Liu M, Shafi M, Rached R, Alfaleh K, et al. Transport modeling of scale inhibitor and scaling ions in an oil-water trunkline with multiple flowlines. ADIPEC. 2025. doi:10.2118/230106-MS.

[40] Li W, Jing J, Sun J, Zhang F, Huang W, Guo Y. Corrosion inhibitor distribution and injection cycle prediction in a high water-cut oil well: a numerical simulation study. Sustainability. 2023;15(7):6289. doi:10.3390/su15076289.

[41] ANSYS. Fluent theory guide. Release 2024 R2; 2024. Available from: https://ansyshelp.ansys.com/public/account/secured?returnurl=/Views/Secured/corp/v242/en/flu_th/flu_th.html.

[42] Bonizzi M, Issa RI. A model for simulating gas bubble entrainment in two-phase horizontal slug flow. International Journal of Multiphase Flow. 2003;29(11):1685-1717. doi:10.1016/j.ijmultiphaseflow.2003.09.001.

[43] Bonizzi M, Andreussi P, Banerjee S. Flow regime independent, high resolution multi-field modelling of near-horizontal gas–liquid flows in pipelines. International Journal of Multiphase Flow. 2009;35(1):34-46. doi:10.1016/j.ijmultiphaseflow.2008.09.001.

[44] Brackbill JU, Kothe DB, Zemach CA. A continuum method for modeling surface tension. Journal of Computational Physics. 1992;100(2):335-354. doi:10.1016/0021-9991(92)90240-Y.

[45] Launder BE, Spalding DB. The numerical computation of turbulent flows. Computer Methods in Applied Mechanics and Engineering. 1974;3:269-289.

[46] Wolfshtein M. The velocity and temperature distribution in one-dimensional flow with turbulence augmentation and pressure gradient. International Journal of Heat and

Mass Transfer. 1969;12(3):301-318. doi:10.1016/0017-9310(69)90012-X.

[47] Jongen T. Simulation and modeling of turbulent incompressible fluid flows [PhD thesis]. Lausanne: École Polytechnique Fédérale de Lausanne (EPFL); 1998. doi:10.5075/EPFL-THESIS-1758.

[48] van Doormaal JP, Raithby GD. Enhancements of the SIMPLE method for predicting incompressible fluid flows. Numerical Heat Transfer. 1984;7:147-163.

[49] Zienkiewicz OC, Nithiarasu P, Codina R, Vázquez M, Ortiz P. The characteristic-based-split procedure: an efficient and accurate algorithm for fluid problems. International Journal for Numerical Methods in Fluids. 1999;31(1):359-392. doi:10.1002/(SICI)1097-0363(19990915)31:1<359::AID-FLD984>3.0.CO;2-7.

[50] Roache PJ. Perspective: a method for uniform reporting of grid refinement studies. Journal of Fluids Engineering. 1994;116(3):405-413. doi:10.1115/1.2910291.

[51] Celik IB, Ghia U, Roache PJ, Freitas CJ. Procedure for estimation and reporting of uncertainty due to discretization in CFD applications. Journal of Fluids Engineering. 2008;130(7):078001. doi:10.1115/1.2960953.

[52] Lopes MFP. Aplicação numérica e experimental de métodos de simulação da camada limite atmosférica para o estudo da acção do vento sobre edifícios [master's dissertation]. Lisbon: Instituto Superior Técnico, Technical University of Lisbon; 2008.

[53] Celik IB. Introductory turbulence modeling. Morgantown (WV): West Virginia University, Mechanical & Aerospace Engineering Department; 1999.

[54] Cazarez-Candia O, Piedra-González S. Modeling of heavy oil-water core-annular upward flow in vertical pipes using the two-fluid model. Journal of Petroleum Science and Engineering. 2017;150:146-153. doi:10.1016/j.petrol.2016.12.004.